Int. J. Solids Structures Vol. 28, No. 6, pp. 669–689, 1991
Printed in Great Britain.

0020-7683/91 $3.00+.00

TOUGHENING AND STRENGTHENING OF CERAMICS REINFORCED BY DILATANT TRANSFORMATIONS AND DUCTILE PARTICLES

DAVID M. STUMP†
Division of Applied Sciences, Harvard University, Cambridge, MA 02138, U.S.A.

(*Received* 10 *March* 1990; *in revised form* 27 *November* 1990)

Abstract—This theoretical study considers the toughening and strengthening of brittle ceramic matrices reinforced by both dilatant phase-transforming particles and ductile crack-bridging particles. Nondimensional toughnesses are calculated as a function of the growth of "long", dominant precut cracks, and nondimensional strengths are calculated as a function of the growth of pre-existing finite cracks. The presence of the dilatant transformations results in peak toughnesses and peak strengths for finite amounts of crack growth. For certain parametric combinations of reinforcements, synergistic interactions may result in peak toughness and strength ratios that exceed substantially the corresponding levels due to the "uncoupled" (i.e. isolated) mechanisms.

INTRODUCTION

The applied mechanics and materials science communities have devoted considerable attention to improving the mechanical properties of normally "fragile" ceramics through the fabrication of novel systems which incorporate small reinforcements within a brittle ceramic matrix. There are three major categories of reinforcements: fibers, phase-transforming particles, and ductile particles. The effects of the individual reinforcement mechanisms on mechanical properties can be substantial. For example, the critical fracture toughnesses, K_{IC}s, of ceramics reinforced by small phase-transforming zirconia particles can often be two to three times those of the unreinforced matrix ceramics (Evans and Cannon, 1986).

This theoretical study considers increases in the critical fracture toughnesses and critical tensile fracture strengths of normally "fragile" ceramics that are reinforced by the *combination* of phase-transforming particles and ductile particles. This combination is of interest for two reasons. First, it has been predicted that in certain instances the mechanisms will interact and provide *synergistic* increases in steady-state toughnesses (Amazigo and Budiansky, 1988). Secondly, a recent theoretical study of resistance curves in partially-stabilized zirconia materials (Stump and Budiansky, 1989a) discovered peak toughnesses that exceed substantially the corresponding steady-state levels. A complementary study of growing finite cracks (Stump and Budiansky, 1989b) found that the transformations also increased the tensile fracture strengths of these materials. Similar peaks in fracture toughnesses and tensile fracture strengths are also expected to occur when phase-transforming particle reinforcements are combined with ductile particle reinforcements. Furthermore, the interaction between the two kinds of reinforcements may result in overall peak toughnesses and strengths which greatly exceed those found in ceramics reinforced with transforming particles alone. It should be noted that combinations of fibers and phase-transforming particles are also expected to exhibit interactions. However, such combinations are not pursued in this study.

The first part of this study reviews toughening and strengthening results for the individual or "isolated" mechanisms. The second portion considers toughening due to the growth of "long" precut cracks in the "combined" material and includes a review of results for steady-state crack growth. The third section examines strengthening during the growth of pre-existing finite cracks in the "combined" material. The final section contains some concluding remarks.

† Present address: E.G.&G. Idaho, P.O. Box 1625, Idaho Falls, ID 83415.

REVIEW OF INDIVIDUAL MECHANISMS

We proceed with concise reviews of toughening and strengthening results for the "isolated" transformation and particulate reinforcement mechanisms. (The two labels, *transformation* and *particulate*, will be used throughout this study to refer respectively to the reinforcing effects of phase-transforming particles and ductile particles.) In the interest of brevity, primary attention is paid to theoretical work, although some experimental results are cited.

Phase-transforming particle reinforcements

Transformation toughening in ceramics was first documented by Garvie *et al.* (1975) and results from the phase transformation of small zirconia particles, typically less than 1 μm in size, that are embedded in a nontransforming ceramic matrix. The high stresses near an advancing crack tip cause a surrounding region of metastable tetragonal-phase zirconia particles to transform to a more stable monoclinic crystal structure. The transformed particles left behind the tip provide a substantial increase in the apparent toughness of the composite.

Transformation toughening has been extensively studied in the applied mechanics literature using the "supercritical" transformation model introduced by Budiansky *et al.* (1983) to treat partially-stabilized zirconia (PSZ). The region of transformed particles is modeled as a continuum that has undergone a permanent "stress-free" transformation dilatation of strength $c_t\theta_p^T$, where c_t is the volume fraction of transforming particles (generally 0.1–0.4), and θ_p^T is the unconstrained particle dilatation (about 0.04). The transformation is assumed to occur "supercritically" (i.e. completely) when the mean stress $\sigma_m = \sigma_{kk}/3$ reaches the critical value σ_m^c. This model seems physically appropriate since individual particles appear either fully transformed or nontransformed and is used exclusively throughout this study.

Steady-state crack growth, wherein the crack faces are bordered by two small-scale transformed regions of height H_T, has been considered by a number of investigators including McMeeking and Evans (1982), Budiansky *et al.* (1983), Rose (1986) and Budiansky and Amazigo (1987). Budiansky and Amazigo (1987) defined the *transformation-toughening* parameter

$$\omega = \frac{Ec_t\theta_p^T}{\sigma_m^c}\left(\frac{1+\nu}{1-\nu}\right) \tag{1}$$

and the plane-strain characteristic length

$$L = \frac{2}{9\pi}\left[\frac{K_m(1+\nu)}{\sigma_m^c}\right]^2 \tag{2}$$

which are also used in this study. Their complete results for the steady-state toughening ratio $\lambda_T^{ss} = K/K_m$ (K is the magnitude of the remote, applied K-field, and $K_{tip} = K_m$ is the critical value for fracture) are shown in Fig. 1, a plot of $(\lambda_T^{ss})^{-1}$ versus the parameter ω. Remarkably, the toughness ratio diverges, that is, "locks up", for $\omega \geqslant \omega_c \approx 30$ (Rose, 1986).

More recently, Stump and Budiansky (1989a) studied the growth of precut semi-finite cracks using the "supercritical" transformation model. It was observed that the toughness ratios of growing cracks, $\lambda_T = K/K_m$, reached maximum values, λ_T^{max}, for finite amounts of nondimensional growth, $\Delta a/L$, from the precut tip positions. The peak toughness ratios are shown in Fig. 1 where $(\lambda_T^{max})^{-1}$ has also been plotted versus toughening parameter ω. Interestingly, "lock-up" of precut cracks occurs at $\omega \approx 20.2$.

The presence of phase-transforming zirconia particles can also increase the tensile fracture strengths of PSZ materials (Marshall, 1986). Transformation strengthening in PSZ has been studied theoretically by Stump and Budiansky (1989b) who employed the

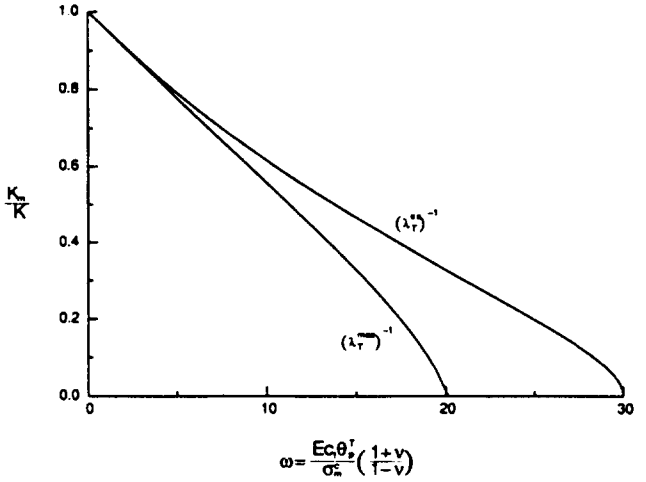

Fig. 1. Reciprocal toughening ratios versus the transformation toughening parameter ω.

"supercritical" transformation model to study the growth of a pre-existing finite crack of length $2a$ under a remote, applied tensile stress σ. The *transformation-toughening* parameter ω and the *crack-length* parameter a/L emerged from their analysis. It was observed that crack growth initiation occurred for values of $\sigma = \sigma_i < \sigma_0$, where $\sigma_0 = K_m/\sqrt{\pi a}$ is the tensile-fracture strength of the unreinforced matrix. However as crack growth occurred, the stress ratios σ/σ_0 climbed and reached peak (or *ultimate*) values σ_{max}/σ_0 for finite amounts of tip advance. Peak strengthening results are shown in Fig. 2, where $(\sigma_{max}/\sigma_0)_T$ has been plotted versus the peak transformation-toughening ratio λ_T^{max} for various values of the *transformation-strengthening* parameter

$$t = \frac{Ec_1\theta_p^T\sqrt{a}}{K_m(1-\nu)} = \frac{\omega}{3}\sqrt{\frac{2a}{\pi L}}. \tag{3}$$

The parameter t is often more convenient than ω and a/L since it is comprised of readily measurable quantities.

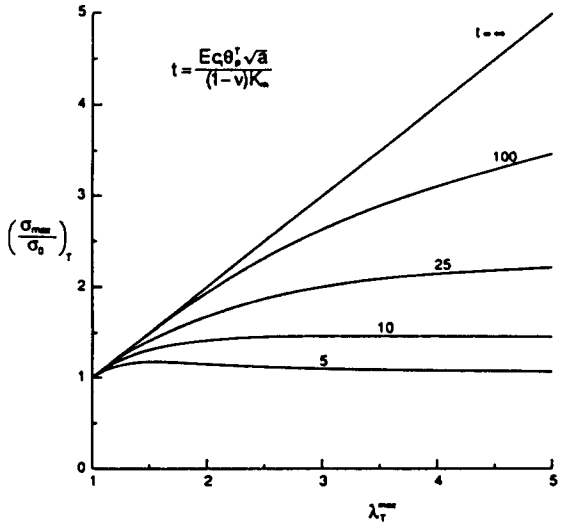

Fig. 2. Peak transformation strengthening ratio $(\sigma_{max}/\sigma_0)_T$ versus λ_T^{max}; various t.

Ductile particle reinforcements

Particulate toughening has been attributed to crack bridging by ductile metal particles embedded in a ceramic matrix (Krystic *et al.*, 1981). Budiansky *et al.* (1988) studied steady-state toughening by assuming a small-scale bridging particle strip of length l_p. Their analysis included rigid ideally-plastic particles which exerted a uniform restraining force S and broke when the *upper* crack face displacement v^+ reached the critical value v_f. (This bridging model is used exclusively throughout this study.) The enhanced toughness was expressed in terms of the *modified* toughness ratio

$$\Lambda_p^{ss} = \frac{K_{ss}}{K_m\sqrt{1-c_p}} \tag{4}$$

where c_p is the ductile-particle volume fraction, the applied $K = K_{ss}$, and the critical K_{tip} for fracture is $K_m\sqrt{1-c_p}$. The square root factor accounts for the decrease in *matrix* crack front due to the presence of the bridging particles. [In the sequel, toughnesses and strengths which involve a $\sqrt{1-c_p}$ factor, and lengths that involve a $(1-c_p)$ factor will be referred to as *modified* quantities.] A J-integral analysis was used to derive the formula

$$\Lambda_p^{ss} = \left[1 + \frac{2Ec_pSv_f}{K_m^2(1-\nu^2)(1-c_p)}\right]^{1/2} \tag{5}$$

where E and ν are the elastic constants of the composite. An additional relation between Λ_p^{ss} and l_p was provided by

$$\Lambda_p^{ss} = 1 + \frac{c_pS}{K_m}\sqrt{\frac{8l_p}{\pi(1-c_p)}} \tag{6}$$

which came directly from a manipulation of stress-intensity factors.

Flinn *et al.* (1989) examined crack growth in Al_2O_3 and found that eqn (5) provided agreement within about a factor of two, while the accuracy of (6) remained uncertain due to the difficulty of obtaining plane strain values of l_p. Nevertheless, the validity of both relations (5) and (6) is assumed for the remainder of this study.

Stump (1989) extended the work of Erdogan and Joseph (1989) and Unswarungsri and Knauss (1988) and studied particulate strengthening by modeling the growth of finite cracks in composites reinforced with rigid ideally-plastic particles. Toughness ratios σ/σ_1, where $\sigma_1 = \sigma_0\sqrt{1-c_p}$ is the modified tensile fracture strength of the unreinforced ceramic, were calculated as a function of the normalized extension $\Delta a/a$ for prescribed values of the steady-state toughness ratio Λ_p^{ss} and the *particulate-strengthening* parameter

$$p = \frac{c_pS}{\sigma_1} = \frac{c_pS\sqrt{\pi a}}{K_m\sqrt{1-c_p}} \tag{7}$$

and reached peak levels σ_{max}/σ_1 at finite amounts of crack growth. Particulate strengthening results are shown in Fig. 3, where $(\sigma_{max}/\sigma_1)_p$ has been plotted versus Λ_p^{ss} for various values of p. For fixed Λ_p^{ss}, σ_{max}/σ_1 increases with p until a plateau level is reached. Based on Flinn *et al.* (1989) estimates for an Al/Al_2O_3 system, critical crack sizes 0.01–1 mm correspond only to the values $p = 0.15$–1.5. Thus, given current levels of strength S, particulate reinforcements are not expected to provide important strengthening effects for "small" critical cracks, despite the fact that the corresponding toughness enhancements can be substantial.

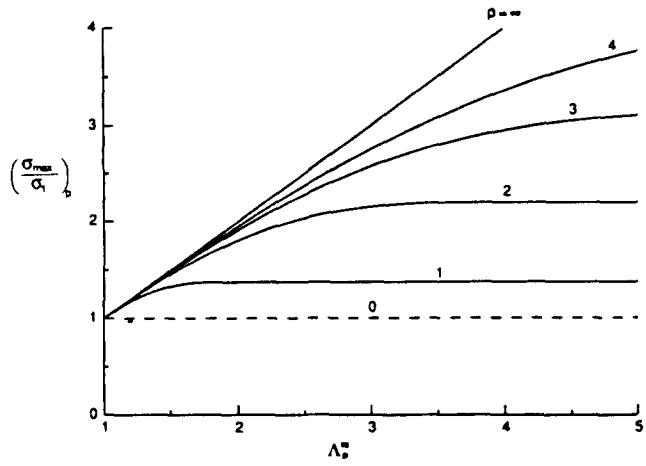

Fig. 3. Peak particulate strengthening ratio $(\sigma_{max}/\sigma_1)_p$ versus Λ_p^{ss}; various p.

TOUGHENING DUE TO COMBINED MECHANISMS

This section considers toughening during the growth of "long", dominant cracks in the "combined" material. Throughout the analysis, the small-scale assumption is made, and the remote and near-tip stresses are given respectively by Mode I K-fields of magnitude K and K_{tip}. We begin with a review of results for steady-state crack growth.

Steady-state crack growth

The combination of transformation and particulate toughening mechanisms may provide an overall toughness that exceeds the simple sum of the "uncoupled" effects since the increased applied K necessary to overcome the bridging particles will simultaneously expand the size of the transformed region. The extra transformed material provides further toughening beyond that due to just the "isolated" mechanisms. In order to assess the effects of the combined mechanisms with respect to the "uncoupled" systems, the component toughness ratios λ_T^{ss} and Λ_p^{ss} due to the individual mechanisms are taken as prescribed material constants.

Amazigo and Budiansky (1988) studied steady-state crack growth by combining supercritical transformations and rigid ideally-plastic bridging particles. The crack faces were bordered by small-scale transformation wakes of height H_s while the tip was bridged by a "Dugdale-like" particle strip of length l_s. The modified steady-state toughness ratio Λ_{ss}, given by the form of (4), was found as a function of the prescribed component toughening ratios λ_T^{ss} and Λ_p^{ss}, and the "natural" coupling parameter

$$\rho = \frac{c_p S(1+\nu)}{\sigma_m^c}. \tag{8}$$

For the limiting values $\rho \to (0, \infty)$, analytical arguments were developed to show that the overall toughness ratios obeyed the formulas

$$\Lambda_{ss} = \lambda_T^{ss}\Lambda_p^{ss} \quad \rho \to \infty \tag{9}$$

$$\Lambda_{ss} = [(\lambda_T^{ss})^2 + (\Lambda_p^{ss})^2 - 1]^{1/2} \quad \rho \to 0. \tag{10}$$

Large values of ρ obey the synergistic product rule relationship (9). Surprisingly, it was found that values of $\rho \approx 1$ yielded overall toughness ratios Λ_{ss} almost as high as those predicted by (9). However, the difficulty in using the parameter ρ is that the values S and σ_m^c are difficult to access and can only be estimated approximately. A more elucidating coupling parameter is provided by the combination

$$\eta = \frac{H_T(1-c_p)}{l_p} \tag{11}$$

where H_T and l_p are the "uncoupled" transformation wake height and bridging segment length. The parameters η and ρ obey the relation

$$\eta = \frac{4\rho^2}{\pi\omega}\left[\frac{(\lambda_T^{ss})^2-1}{(\Lambda_p^{ss}-1)^2}\right] \tag{12}$$

where λ_T^{ss} and ω are assumed to be related via Fig. 1. The formulas (9) and (10) continue to apply for the limiting values $\eta \to (0, \infty)$. Interestingly, it was observed that in some instances η as small as 0.1 resulted in values of Λ_{ss} almost as high as those given by the product rule (9). This is an important result since transformation wake heights H_T do not usually exceed 50 μm, while bridge lengths l_p may be many times longer. [Krystic (1983) reported a bridge length in excess of 200 μm for the Al/Al_2O_3 system.] Thus, synergistic interactions may be possible for mixtures of existing systems of dilatantly transforming particles and ductile bridging particles.

We begin the study of "long", dominant precut cracks by considering crack growth initiation. Next, the overall toughness ratio is calculated as a function of normalized crack advance. Particular attention is paid to how the two mechanisms interact to determine the overall resistance. The presence of dilatant transformations results in peak toughening phenomena for finite amounts of growth from the precut tip positions.

Crack growth initiation

A precut crack at the instant of crack growth initiation is shown schematically in Fig. 4. The crack tip is surrounded by a region of transformed material while the front is blocked by nondeformed particles. Ductile particles lying in the crack plane behind the tip have been severed by the introduction of the crack so that there is no initial bridging. Thus, crack growth initiation depends on just the effects of the applied K and the transformations. However, as was discussed by Budiansky *et al.* (1983), the transformations do not effect K_{tip} of the precut crack so that near and far K-fields coincide (i.e. $K = K_{tip}$).

At the instant of crack growth initiation, K_{tip} has just reached the critical modified value $K_m\sqrt{1-c_p}$, while σ_m along the exterior of the transformed region is equal to σ_m^c. The coordinates of points on the *upper* half of the surrounding boundary are given in terms of a complex variable $z = x+iy$ by

$$z(\theta) = R(\theta)[\cos(\theta) + i\sin(\theta)] \quad 0 \leqslant \theta \leqslant \pi \tag{13}$$

where $R(\theta)$ is the boundary-radius vector. (The shape of the transformed region is assumed Mode-I symmetric throughout the analysis.) The initial-boundary shapes found by Stump and Budiansky (1989a) for various values of the parameter ω continue to apply if the characteristic length L, given by (2), is replaced with the modified form $L_1 = L(1-c_p)$.

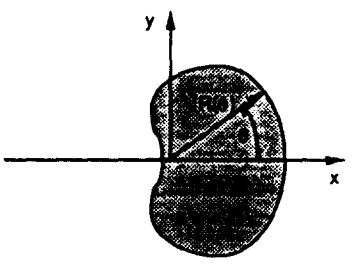

Fig. 4. Crack growth initiation in the combined material.

Resistance curves

As crack growth occurs, the advancing tip transforms "fresh" material, while leaving behind wake regions of permanently transformed material and a strip of bridging particles. The instantaneous toughness depends on both the shape of the surrounding transformed region and the effects of the bridging strip. We begin by detailing the model used to treat the transformed region.

The three-piece boundary model of Stump and Budiansky (1989a) is used to describe the evolution of the transformed region for a crack that is advancing by a series of small growth increments δa. The upper half of a crack that has advanced by the overall amount Δa is shown in Fig. 5. The transformation boundary is divided into three segments: the active, passive, and residual. Along the active segment MN, material has just transformed according to the σ_m^c criterion. The points on the current active segment are described in terms of translating crack-tip coordinates by the complex form

$$z(\theta) = R(\theta)[\cos(\theta) + i\sin(\theta)] \quad 0 \leqslant \theta \leqslant \alpha \tag{14}$$

where $R(\theta)$ is the active-segment radius vector and α is an unknown angle. The residual segment OP is that portion of the initial transformation boundary left behind with the first increment of crack growth. The passive segment is a growth dependent piece that connects the end of the residual segment, O, with the end of the active segment, N. In the limit of infinitesimal crack growth, the passive piece provides a smooth connection between the active and residual pieces. For a crack which is advancing by small finite growth increments, the passive segment is approximated by a series of straight-line segments that run through the ends of the previous active segments, while always providing a smooth connection to the residual and current active pieces. Finally, we note that the coordinates of boundary in the interval $\alpha < \theta < \pi$ can also be described with the form of (14) by having $R(\theta)$ connect the current tip with the known passive and residual segments.

The formation of the bridging strip is divided into two distinct phases. Immediately after the start of growth, the crack-opening displacement (COD) within the strip has not reached the critical value $2v_f$ so that all of the particles left behind the advancing tip remain intact. Throughout this initial-growth phase, the bridge length l is equal to the tip advance Δa, and the change in strip length δl during each small growth increment is given directly by δa. When Δa reaches a special value l_c, the critical COD is achieved at the end of the strip and particle rupture commences. The crack continues to advance in a stage of generalized growth as shown in Fig. 5, where the bridge length l varies as the critical COD is maintained at the strip end. Since the rehealing of particles cannot occur, the condition $\delta l \leqslant \delta a$ must not be violated throughout growth. The equations governing generalized growth are developed in Appendix A, Part I and are also adapted to handle the initial growth phase.

"R-curves", that is, plots of the toughness ratio Λ versus the nondimensional crack advance $\Delta a/L_1$, are shown in Figs 6 and 7 for $\omega = 5$ and 10 ($\lambda_T^{max} = 1.27$ and 1.81), $\Lambda_p^u = 2$, and a variety of ρ. The treatment of the limiting values $\rho = (0, \infty)$ is discussed in Appendix A, Part II. Maximum ratios, Λ_{max}, occur for finite amounts of crack growth and are discussed further below. After the cracks have grown a very long way, the Λs approach the corresponding steady-state Λ_{ss}s found by Amazigo and Budiansky (1988). Some bridge lengths l/L_1 corresponding to the R-curves of Fig. 6 are plotted versus $\Delta a/L_1$ in Fig. 8. The critical values l_c/L_1 at which particle rupture commences are marked by the departure of

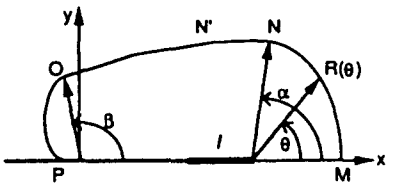

Fig. 5. Generalized growth model of combined material crack.

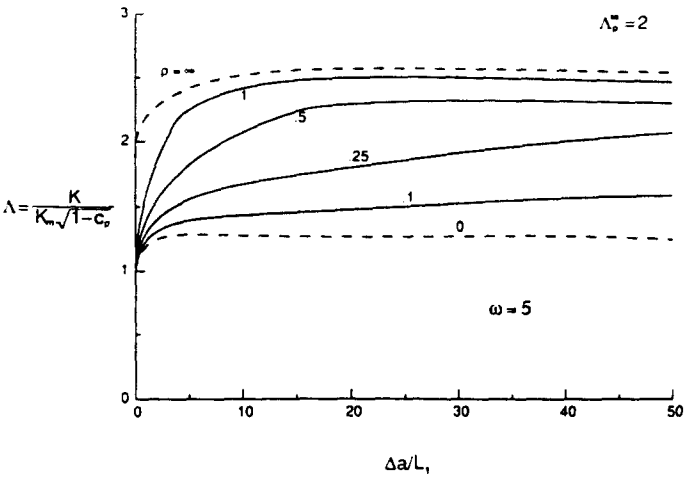

Fig. 6. Toughness ratios Λ versus $\Delta a/L_1$; $\Lambda_\rho^\infty = 2$, $\omega = 5$, various ρ.

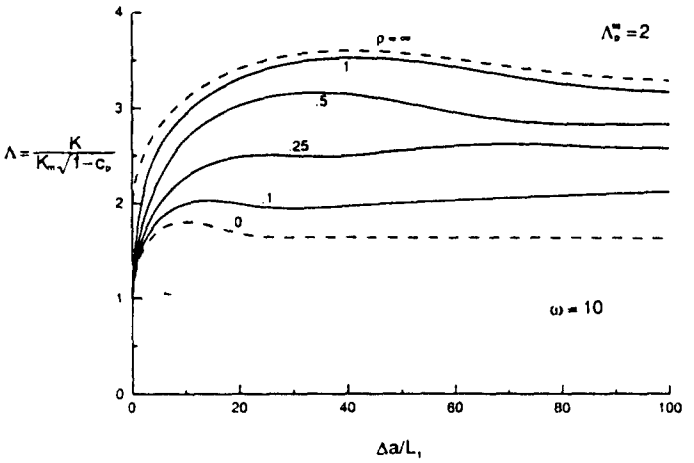

Fig. 7. Toughness ratios Λ versus $\Delta a/L_1$; $\Lambda_\rho^\infty = 2$, $\omega = 10$, various ρ.

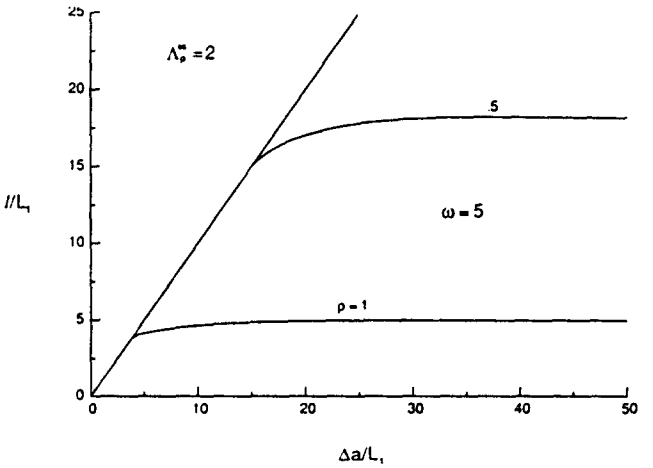

Fig. 8. Bridge lengths l/L_1 versus $\Delta a/L_1$; $\Lambda_\rho^\infty = 2$, $\omega = 5$, various ρ.

the curves from the straight line $l/L_1 = \Delta a/L_1$. Notice, the l/L_1s remain fairly constant once particle rupture begins.

The Λ_{max}s depend on the *interaction* between the particulate and transformation mechanisms. For "large" ρ, strong interactions produce Λ_{max}s much greater than the Λ_{ss}s, while the Λ_{max}s for "small" ρ just barely exceed the corresponding Λ_{ss}s. This dependence on ρ

reflects the influence of the bridging particles in amplifying substantially the peak in the transformation toughness component. For "strong" interactions, the bridging particles provide substantial reinforcement "early" in growth, that is, prior to the peak in transformation toughness. The extra K necessary to overcome the bridging strip expands the transformation region, thus causing Λ_{max} to exceed considerably the corresponding Λ_{ss}. For "weak" interactions, particulate reinforcement only contributes significantly when the crack has advanced beyond the region of peak transformation toughening. Thus, these cracks have already approached their steady-state configuration when significant interaction occurs, and Λ_{max} just barely exceeds Λ_{ss}.

We conclude this section with Figs 9–11, plots of Λ_{max}s versus λ_T^{max} for a variety of ρ and the values $\Lambda_p^{ss} = 2$, 3 and 4. Selected values of the alternative coupling parameter η are marked by the small triangles. When compared with the steady-state results of Amazigo and Budiansky (1988), it is evident that synergistic interactions can occur for even smaller values of η than has been previously thought. It is particularly noteworthy that slight

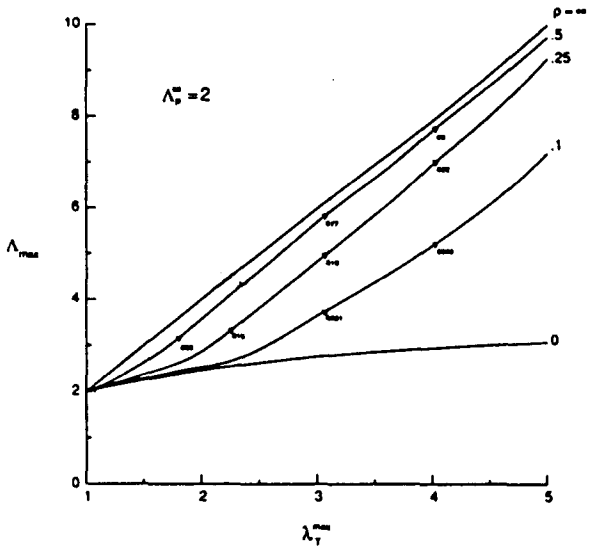

Fig. 9. Peak toughness ratios Λ_{max} versus λ_T^{max}; $\Lambda_p^{ss} = 2$, various ρ.

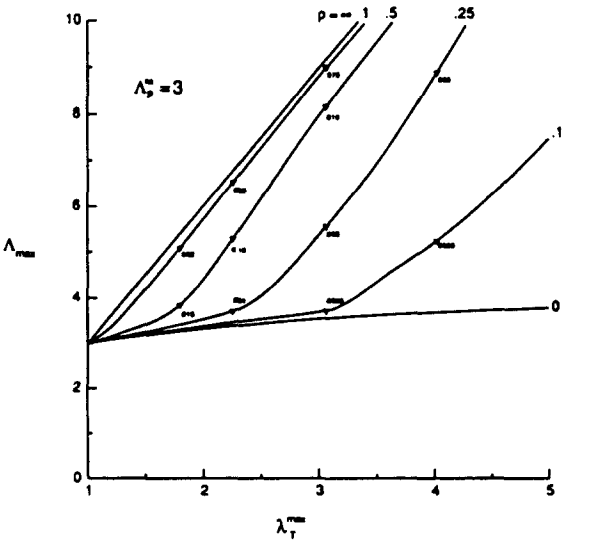

Fig. 10. Peak toughness ratios Λ_{max} versus λ_T^{max}; $\Lambda_p^{ss} = 3$, various ρ.

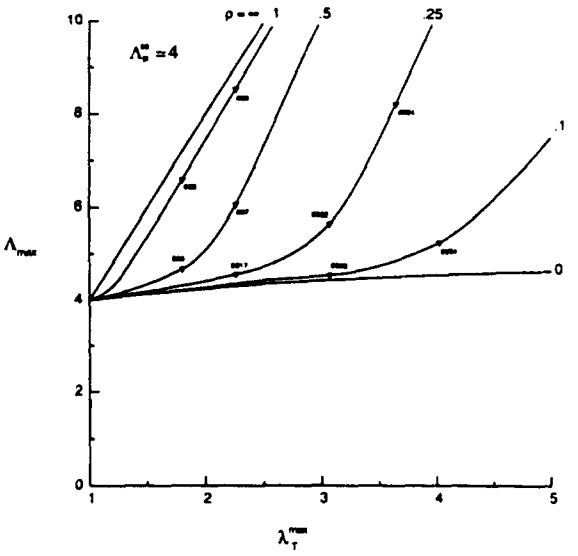

Fig. 11. Peak toughness ratios Λ_{max} versus λ_T^{max}; $\Lambda_\rho^{ss} = 4$, various ρ.

changes in η can produce very large increases in toughness. In the limit the parameters $(\rho, \eta) \to \infty$, the approximate product rule relationship

$$\Lambda_{max} \approx \lambda_T^{max} \Lambda_\rho^{ss} \quad (\rho, \eta) \to \infty \tag{15}$$

applies, while for the limit $(\rho, \eta) \to 0$, Λ_{max} coincides with Λ_{ss} and the exact formula

$$\Lambda_{max} = [(\lambda_T^{ss})^2 + (\Lambda_\rho^{ss})^2 - 1]^{1/2} \quad (\rho, \eta) \to 0 \tag{16}$$

remains in effect. (The toughening ratios λ_T^{max} and λ_T^{ss} are assumed to be related by Fig. 1.)

STRENGTHENING DUE TO COMBINED MECHANISMS

This section considers strengthening during the growth of precut, finite cracks in the combined material. We begin with an analysis of crack growth initiation, followed by the treatment of growing cracks. This section is concluded with an examination of synergistic strengthening.

Crack growth initiation

A precut crack of length $2a$ at the instant of crack growth initiation is represented schematically in Fig. 12. The remote, nonzero, plane-strain stresses are

$$\sigma_{22} = \sigma, \quad \sigma_{33} = \sigma \tag{17}$$

while the asymptotic near-tip stresses obey Mode-I K-fields of magnitude K_{tip}. The crack fronts are blocked by nondeformed ductile particles, so that crack-growth initiation occurs when the effects of the applied stress $\sigma = \sigma_i$ and the transformations cause K_{tip} to reach the critical modified value $K_m\sqrt{1 - c_p}$. At this instant σ_m is equal to the critical value σ_m^c just

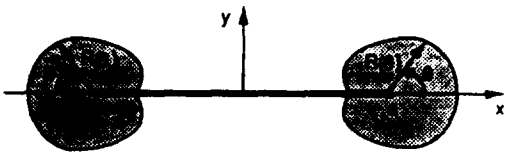

Fig. 12. Precut finite crack at the instant of crack growth initiation.

outside both the right and left transformed regions. The coordinates on the upper halves of the right (+) and left (−) boundaries are given in terms of crack-tip polar coordinates by the complex form

$$z_{+,-}(\theta) = \pm R(\theta)[\cos(\theta) \pm i \sin(\theta)] \pm a \quad 0 \leqslant \theta \leqslant \pi \tag{18}$$

where $R(\theta)$ is the bounary-radius vector and θ is measured as shown in Fig. 12. The crack growth initiation results of Stump and Budiansky (1989b) for transformation strengthening are adapated to describe the "combined" material by replacing the quantities σ_0 and L with the modified forms σ_1 and L_1.

Strengthening curves

As the crack tips advance symmetrically, "fresh" material is transformed while wake regions of previously transformed material and strips of bridging particles are left behind. The active-passive-residual boundary model is adapted to describe the evolution of the transformed regions for a series of prescribed growth increments δa. The points on the current active segments are given in terms of translating crack-tip coordinates by

$$z_{+,-}(\theta) = \pm R(\theta)[\cos(\theta) \pm i \sin(\theta)] \pm c \quad 0 \leqslant \theta \leqslant \alpha \tag{19}$$

where $R(\theta)$ is the current boundary radius vector, the right crack-tip position $c = a + \Delta a$, and α is an unknown angle that varies with each growth increment. The form of (19) also describes the transformed region boundaries in the interval $\alpha \leqslant \theta \leqslant \pi$ by having $R(\theta)$ connect the tips with the known coordinates of the passive and residual segments.

The development of the bridging strips is again divided into initial and generalized growth phases. During initial growth, the advancing tips leave behind intact bridging particles so that the strip ends at $\pm d$ remain fixed at the precut tip positions $\pm a$. Thus, the instantaneous strip length $l = c - d$ is given by the overall tip advance Δa, while the incremental change in strip length δl is equal to the growth increment δa. When the crack has grown far enough that the critical COD is reached at $\pm a$, generalized growth begins as particle rupture commences. Throughout this stage, the strip ends trail the advancing tips as the critical COD is maintained. Since the rehealing of ruptured particles is not allowed, the condition $\delta l \leqslant \delta a$ cannot be violated during crack growth. The equations governing generalized growth are developed in Appendix B, Part I and are specialized to handle initial growth.

"*S*-curves", that is, plots of σ/σ_1 versus the crack extension $\Delta a/L_1$, are shown in Figs 13–15 for $\omega = 10$, $\Lambda_p^u = 2$, a variety of ρ, and the values of the modified crack-length parameter $a/L_1 = 5000, 50, 5$. The treatment of the limiting values $\rho = (0, \infty)$ is discussed in Appendix B, Part II. The maximum stress ratios, σ_{max}/σ_1s, occur at finite amounts of growth and depend on the interaction between mechanisms, since throughout crack growth the "nominal" K, given by $\sigma\sqrt{\pi c}$, must overcome the combined K_{tip} due to the transformations, bridging strips, and inherent tip resistances.

For "strong" interactions (i.e. $\rho > 1$), the particulate resistance becomes important just after the start of growth and amplifies the effects of the transformations. For "long" cracks (i.e. large a/L_1), the transformations alone have the most effect, and the interaction with the "strong" bridging strips results in the highest values of σ_{max}/σ_1. "Strong" interactions also cause substantial increases in the σ_{max}/σ_1s for "short" cracks (i.e. small a/L_1). However, since the transformation effects are weaker, these σ_{max}/σ_1s are much lower than those of the "long" cracks.

For "weak" interactions (i.e. $\rho \approx 0$), the bridging strips only become important after the cracks have grown a very long way. Thus, the σ/σ_1s depend mainly on the transformations with any interaction only taking place after the "nominal" K due to the applied tensile stress dominates all other contributions. These σ_{max}/σ_1s are given approximately by the renormalized form of Stump and Budiansky's (1989b) transformation-strengthening results.

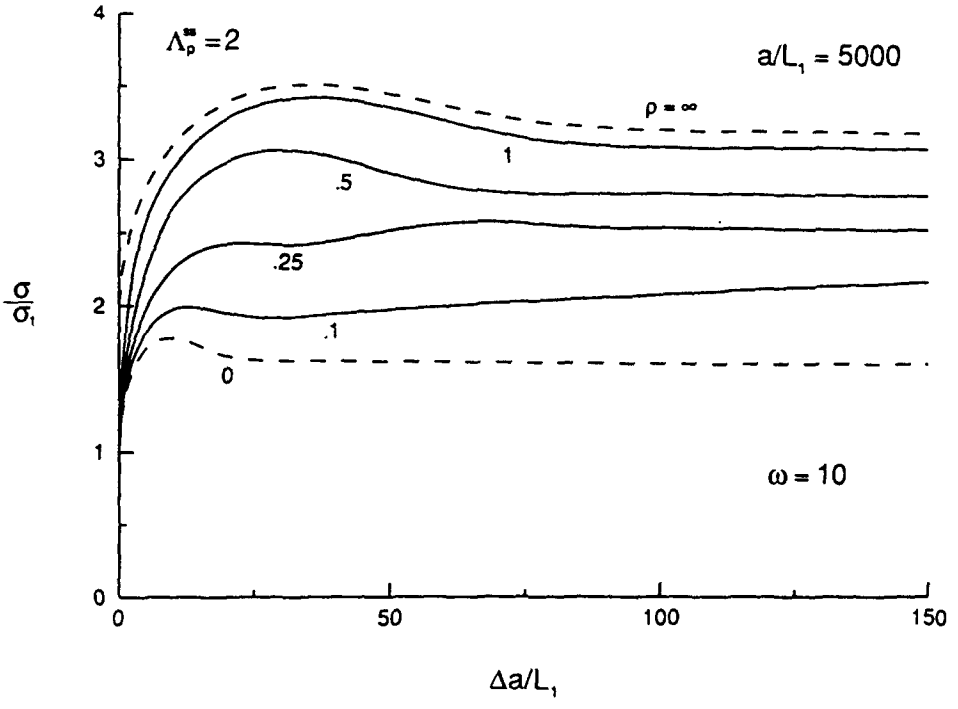

Fig. 13. Stres ratios σ/σ_1 versus $\Delta a/L_1$; $\omega = 10$, $\Lambda_\rho^{\infty} = 2$, $a/L_1 = 5000$, various ρ.

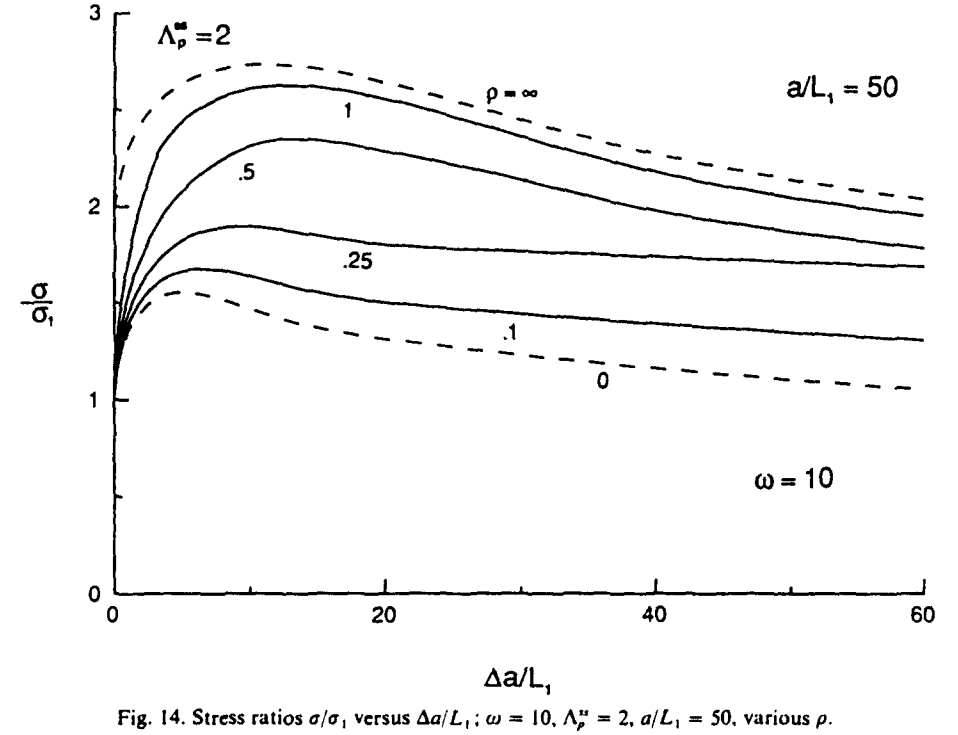

Fig. 14. Stress ratios σ/σ_1 versus $\Delta a/L_1$; $\omega = 10$, $\Lambda_\rho^{\infty} = 2$, $a/L_1 = 50$, various ρ.

The large number of independent parameters in the combined strengthening problem make it difficult to present peak strengthening results in a single graph. However to illustrate the effect of the modified crack-length parameter a/L_1, σ_{max}/σ_1s are plotted versus the prescribed peak *transformation* stress-ratio $(\sigma_{max}/\sigma_1)_T$ in Figs 16 and 17 for $a/L_1 = 5000$ and 50, a variety of ρ, and $\Lambda_\rho^{\infty} = 2$. The abscissa values of $(\sigma_{max}/\sigma_1)_T$ are obtained by replacing σ_0 and L with their modified forms and using the *modified transformation-strengthening* parameter

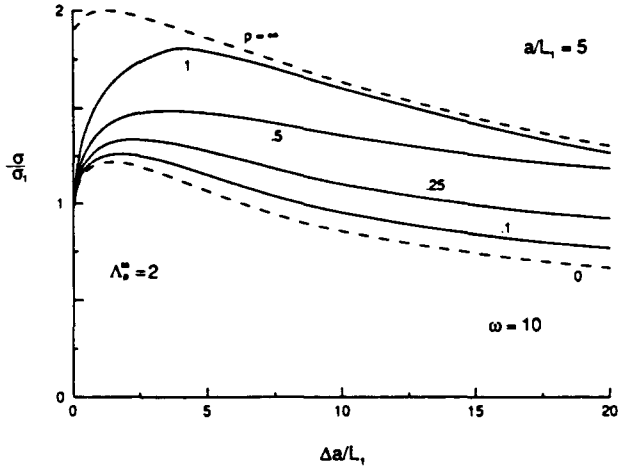

Fig. 15. Stress ratios σ/σ_1 versus $\Delta a/L_1$; $\omega = 10$, $\Lambda_\rho^\infty = 2$, $a/L_1 = 5$, various ρ.

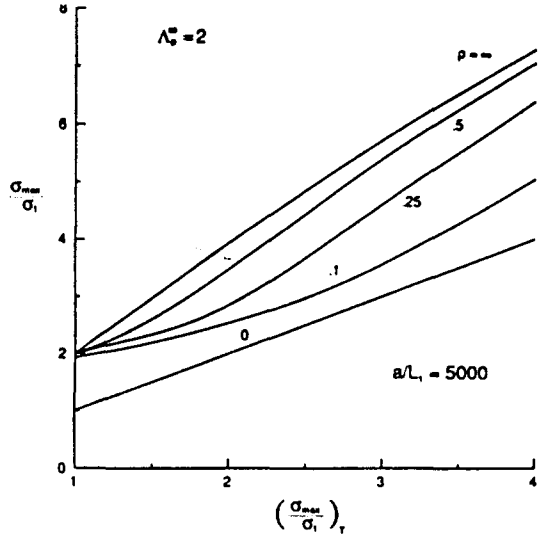

Fig. 16. Peak stress ratios σ_{max}/σ_1 versus $(\sigma_{max}/\sigma_1)_T$; $\Lambda_\rho^\infty = 2$, $a/L_1 = 5000$, various ρ.

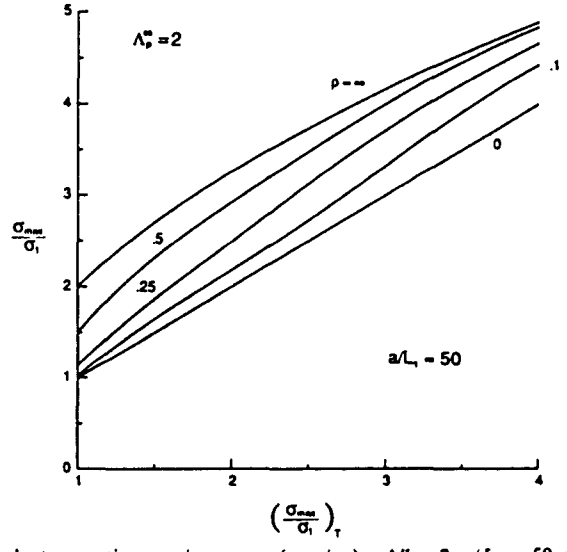

Fig. 17. Peak stress ratios σ_{max}/σ_1 versus $(\sigma_{max}/\sigma_1)_T$; $\Lambda_\rho^\infty = 2$, $a/L_1 = 50$, various ρ.

Table 1. "Synergism" ratio as a function of a/L_1 and ρ. $\Lambda_p^{cr} = 2$, $\lambda_T^{max} = 1.8$ ($\omega = 10$)

	ρ					
a/L_1	∞	1	0.5	0.25	0.1	0
∞	1	0.978	0.879	0.727	0.680	1
5000	0.987	0.963	0.864	0.730	0.700	1
500	0.956	0.930	0.840	0.739	0.783	1
50	0.883	0.880	0.881	0.967	1.04	1
5	0.990	1.05	1.10	1.07	1.03	1

$$t_1 = \frac{Ec_t\theta_p^T\sqrt{a}}{K_m(1-\nu)\sqrt{1-c_p}} = \frac{\omega}{3}\sqrt{\frac{2}{\pi}\frac{a}{L_1}} \tag{20}$$

in re-interpreting Fig. 2. Notice, for given ρ, the σ_{max}/σ_1s of the "short" crack ($a/L_1 = 50$) are much lower than those of the "long" crack ($a/L_1 = 5000$).

Finally, we consider synergistic strengthening. In the previous section, it was shown that in the limit $\rho \to \infty$, the Λ_{max}s of "combined" material are given approximately by the *product* of the uncoupled toughness ratios, Λ_p^{cr} and λ_T^{max}. It is instructive to determine if a similar product rule also holds between strength ratios when $\rho \to \infty$. Table 1 shows the "synergism" ratio

$$\frac{\sigma_{max}/\sigma_1}{(\sigma_{max}/\sigma_1)_T(\sigma_{max}/\sigma_1)_p} \tag{21}$$

as a parametric function of various values of the parameters a/L_1 and ρ given prescribed *toughness* ratios $\lambda_T^{max} = 1.81$ ($\omega = 10$) and $\Lambda_p^{cr} = 2$. The values of $(\sigma_{max}/\sigma_1)_T$ were obtained by re-interpreting the results of Fig. 2, while values of $(\sigma_{max}/\sigma_1)_p$ were calculated from Fig. 3 via the relation

$$p = \frac{c_p S}{\sigma_1} = \frac{\rho}{3}\sqrt{\frac{2a}{L_1}}. \tag{22}$$

Values close to unity in Table 1 indicate an approximate product rule relationship. Surprisingly, the "synergism" ratio can exceed unity for small to moderate a/L_1. This is a result of the rapid drop off in $(\sigma_{max}/\sigma_1)_T$ for small cracks, see the small t results in Fig. 2. When reviewing Table 1, it should be remembered that although an approximate product rule occurs for a wide range of a/L_1, the overall tensile fracture strength increases are only substantial (i.e. σ_{max}/σ_1s > 2) when both the "isolated" particulate and transformation mechanisms provide significant strengthening. Synergism tables constructed for other parameter values show similar trends.

CONCLUDING REMARKS

The combination of dilatantly-transforming particle reinforcements and ductile particles reinforcements may improve substantially the fracture toughnesses and tensile fracture strengths of normally "fragile" ceramics. For "long" dominant cracks, synergism may be present for mixtures existing uncoupled systems that have bridge lengths l_p which are no longer than 10 times the transformation wake heights H_T. Based on realistic estimates of the transformation-toughening parameter $0 \leqslant \omega \leqslant 15$, the maximum toughness ratios, Λ_{max}, of the combined material may exceed previous steady-state toughness predictions (Amazigo and Budiansky, 1988) by up to 50%. Composites containing "long" pre-existing, finite cracks and "strong" interactions may experience substantial increases in tensile

fracture strengths. However, the presence of "short" cracks or "weak" interactions are not expected to improve strengths much.

Acknowledgements—The advice and guidance of Professor B. Budiansky is gratefully appreciated. This work was partially supported by the DARPA University Research Initiative (Subagreement P.O. # VB38639-0 with the University of California, Santa Barbara, ONR Prime Contract N00014-86-K-0753), the Office of Naval Research (Contract N00014-84-K-0510), and the Division of Applied Sciences, Harvard University. The support of the National Science Foundation Graduate Fellowship program is also acknowledged.

REFERENCES

Amazigo, J. C. and Budiansky, B. (1988). Interaction of particulate and transformation toughening. *J. Mech. Phys. Solids* **34**, 581–595.

Budiansky, B. and Amazigo, J. C. (1987). Steady-state crack growth in supercritically transforming materials. *Int. J. Solids Structures* **23**, 751–756.

Budiansky, B., Amazigo, J. C. and Evans, A. G. (1988). Small-scale bridging and the fracture toughness of particulate reinforced ceramics. *J. Mech. Phys. Solids* **36**, 167–188.

Budiansky, B., Hutchinson, J. W. and Lambropoulos, J. C. (1983). Continuum theory of dilatant transformation toughening materials. *Int. J. Solids Structures* **19**, 337–356.

Erdogan, F. and Joseph, P. J. (1989). Toughening of ceramics through crack-bridging particles. *J. Am. Cer. Soc.* **72**, 262–270.

Evans, A. G. and Cannon, R. (1986). Toughening of brittle solids by martensitic transformations. *Acta Met.* **34**, 761–803.

Flinn, B., Rühle, M. H. and Evans, A. G. (1989). *Toughening of Al_2O_3 by Al Particles*. University of California, Santa Barbara.

Garvie, R. C., Hannink, R. H. and Pascoe, R. T. (1975). Ceramic steel. *Nature* **258**, 703–704.

Krystic, D. (1983). On the fracture of brittle-matrix/ductile-particle composites. *Phil. Mag. A* **48**, 695–708.

Krystic, V. D., Nicholson, P. S. and Hoagland, R. G. (1981). Toughening of glasses by metallic particles. *J. Am. Cer. Soc.* **64**, 499–504.

Marshall, D. B. (1986). Strength characteristics of transformation toughened zirconia. *J. Am. Cer. Soc.* **69**, 173–180.

McMeeking, R. M. and Evans, A. G. (1982). Mechanics of transformation toughening in brittle materials. *J. Am. Cer. Soc.* **65**, 242–246.

Muskhelishvili, N. I. (1953). *Some Basic Problems of the Mathematical Theory of Elasticity*. Noordhoff, Gronigen.

Rose, L. R. F. (1986). The size of the transformed zone during steady-state cracking in transformation toughened materials. *J. Mech. Phys. Solids* **34**, 609–616.

Stump, D. M. (1989). Ph. D. Thesis, Harvard University.

Stump, D. M. and Budiansky, B. (1989a). Crack growth resistance in transformation toughened ceramics. *Int. J. Solids Structures* **25**, 635–646.

Stump, D. M. and Budiansky, B. (1989b). Finite cracks in transformation-toughened ceramics. *Actra Met.* **37**, 3297–3304.

Tada, H., Paris, P. and Irwin, G. (1985). *The Stress Analysis of Cracks Handbook*. Del Research, St Louis.

Ungswarungsri, T. and Knauss, W. G. (1988). A nonlinear analysis of an equilibrium craze. Part I—Problem formulation, Part II—Simulations of craze and crack growth. *J. Appl. Mech.* **55**, 41–58.

APPENDIX A: ANALYSIS FOR SEMI-INFINITE CRACKS

In part I, the governing equations for growing finite cracks are developed for nonzero, finite values of the interaction parameter ρ. In part II, these equations are specialized for the limiting values $\rho = (0, \infty)$.

Part I: Equation development

Throughout generalized growth, the combined effects of the applied K, the bridging strip, and the transformations maintain σ_m at σ_m^c along the active segment of the transformation boundary while holding K_{tip} at $K_m\sqrt{1-c_\rho}$ and $v^+(-l)$, the upper crack face displacement at the end of the strip as measured from the tip, at v_f. We make use of complex stress potential methods (Muskhelishvili, 1953) and note the following formulas in terms of an overall potential $\phi(z)$,

$$\sigma_m = \frac{4(1+\nu)}{3}\,\mathrm{Re}\left(\frac{\partial\phi}{\partial z}\right) \tag{A1}$$

$$v^+(-l) = \frac{2(1-\nu^2)}{E}\,\mathrm{Im}\,[\phi(-l)]_-^+ \tag{A2}$$

$$K_{tip} = \lim_{x\to 0} 2\sqrt{2\pi x}\,\frac{\partial\phi}{\partial x} \quad x > 0 \tag{A3}$$

where z is measured from the current crack tip. Here, Re and Im denote the real and imaginary parts of a complex quantity, and the brackets indicate the jump in ϕ across the crack faces. The overall potential $\phi(z)$ is equal to the sum of potentials due to the individual effects. According to Amazigo and Budiansky (1988), the potentials due to the applied K and the transformations are

$$\phi_K(z) = K\sqrt{\frac{z}{2\pi}} \tag{A4}$$

$$\phi_T(z) = -\frac{Ec_t\theta_p^T}{6\pi(1-\nu)}\oint \log(\sqrt{z}+\sqrt{z_0})\,dy_0 \tag{A5}$$

where the integral of (A5) is carried out in a counter-clockwise direction over the points z_0 on the exterior of the *entire* transformed region. Tada *et al.* (1985) list the potential for a "Dugdale-like" particle strip of strength c_pS and length l as

$$\phi_p(z) = -\frac{c_pS}{\pi}\left\{\sqrt{lz} - \frac{i}{2}(z+l)\log\left(\frac{\sqrt{z}-i\sqrt{l}}{\sqrt{z}+i\sqrt{l}}\right)\right\}. \tag{A6}$$

The branch cuts for all square-root and log functions are taken along the negative x-axis. The substitution of $\phi = \phi_K+\phi_T+\phi_p$ into eqns (A1)–(A3) then provides

$$\sigma_m = \frac{K(1+\nu)}{3}\sqrt{\frac{2}{\pi}}\,\mathrm{Re}\,\frac{1}{\sqrt{z}} - \frac{Ec_t\theta_p^T}{9\pi}\left(\frac{1+\nu}{1-\nu}\right)\oint \mathrm{Re}\,\frac{1}{\sqrt{z}(\sqrt{z}+\sqrt{z_0})}\,dy_0 - \frac{4c_pS(1+\nu)}{3\pi}\left\{\mathrm{Re}\sqrt{\frac{l}{z}} + \tfrac{1}{2}\,\mathrm{Im}\log\left(\frac{\sqrt{z}-i\sqrt{l}}{\sqrt{z}+i\sqrt{l}}\right)\right\} \tag{A7}$$

$$v^+(-l) = \frac{4(1-\nu^2)}{E}\left\{K\sqrt{\frac{l}{2\pi}} - \frac{c_pSl}{\pi}\right\} - \frac{c_t\theta_p^T(1+\nu)}{3\pi}\oint \mathrm{Im}\log\left(\frac{\sqrt{z_0}+i\sqrt{l}}{\sqrt{z_0}-i\sqrt{l}}\right)dy_0 \tag{A8}$$

$$K_{tip} = K - c_pS\sqrt{\frac{8l}{\pi}} - \frac{Ec_t\theta_p^T}{6(1-\nu)}\sqrt{\frac{2}{\pi}}\oint \mathrm{Re}\,\frac{1}{\sqrt{z_0}}\,dy_0. \tag{A9}$$

The governing equation for the active boundary is formulated by allowing z to approach $z(\theta)$, given by (14), from the exterior of the transformed region while setting $\sigma_m = \sigma_m^c$. The assertion of the critical conditions $K_{tip} = K_m\sqrt{1-c_p}$ and $v^+(-l) = v_f$ then provides two constraints. By introducing the nondimensional coordinates l/L_1 and $Z = z/L_1$, where $L_1 = L(1-c_p)$, the parameters ρ and ω, and the modified toughness ratio Λ, we derive the nondimensionalized equations

$$1 = \Lambda\,\mathrm{Re}\,\frac{1}{\sqrt{Z(\theta)}} - \frac{\omega}{9\pi}\int_{-\pi}^{\pi} M(\theta,\theta')\frac{d}{d\theta'}\left[\frac{R(\theta')\sin(\theta')}{L_1}\right]d\theta' - \frac{2\rho}{3\pi}\left\{2\,\mathrm{Re}\sqrt{\frac{l/L_1}{Z(\theta)}} + \mathrm{Im}\log\left(\frac{\sqrt{Z(\theta)}-i\sqrt{l/L_1}}{\sqrt{Z(\theta)}+i\sqrt{l/L_1}}\right)\right\} \quad \theta \leqslant \alpha \tag{A10}$$

$$w_f = \Lambda\sqrt{\frac{l}{L_1}} - \frac{2\rho l}{3\pi L_1} - \frac{\omega}{18\pi}\int_{-\pi}^{\pi}\mathrm{Im}\log\left(\frac{\sqrt{Z(\theta)}+i\sqrt{l/L_1}}{\sqrt{Z(\theta)}-i\sqrt{l/L_1}}\right)\frac{d}{d\theta}\left[\frac{R(\theta)\sin(\theta)}{L_1}\right]d\theta \tag{A11}$$

and

$$1 = \Lambda - \frac{4\rho}{3\pi}\sqrt{\frac{l}{L_1}} - \frac{\omega}{9\pi}\int_{-\pi}^{\pi}\mathrm{Re}\,\frac{1}{\sqrt{Z(\theta)}}\frac{d}{d\theta}\left[\frac{R(\theta)\sin(\theta)}{L_1}\right]d\theta \tag{A12}$$

where

$$M(\theta,\theta') = \mathrm{Re}\,\frac{1}{\sqrt{Z(\theta)}(\sqrt{Z(\theta)}+\sqrt{Z(\theta')})} \tag{A13}$$

and

$$w_f = \frac{Ev_f}{6(1-\nu)L_1\sigma_m^c}. \tag{A14}$$

Since Λ_p^u is taken as a prescribed material constant, the combination of (2), (5), (8), and (A14) provides the additional relation

$$(\Lambda_p^u)^2 = 1 + \frac{8\rho w_f}{3\pi} \tag{A15}$$

which is used to fix the left side of (A11). Here, we have assumed that E and ν, the elastic constants of the composite, are equal to the *matrix* values.

Growing cracks were handled in the following manner for prescribed values of Λ_p^u, the parameters ρ and ω (λ_T^{max} via Fig. 1), and a series of small finite growth increments $\delta a/L_1$. The equations (A10) and (A12) [a nonlinear

integral equation and constraint for the nondimensional active-boundary radius $R(\theta)/L_1$ and the overall toughness ratio Λ] were enforced throughout crack growth. During the initial growth state, l/L_1 was set equal to the total crack advance $\Delta a/L_1$, and the restriction (A11) was not enforced. Once the right side of (A11) reached the critical value w_f, l/L_1 was allowed to vary, and (A11) was enforced during subsequent growth increments. The numerical solution procedure for the function $R(\theta)/L_1$ and the scalars Λ, l/L_1, and α is described in Appendix C, Part I. After each increment, the condition $\delta l/L_1 \leqslant \delta a/L_1$ was checked to ensure a physically meaningful solution.

Part II: Limiting values of the interaction parameter

In the limit $\rho = 0$, the bridging particles only provide reinforcement when the crack has achieved its steady-state configuration so that $\Lambda_{max} = \Lambda_{ss}$. Thus during growth from the precut position, Λ depends on just the applied K and the transformations. Setting $\rho = 0$ in (A10) and (A12) and eliminating (A11) provides equations which are similar in form to those describing transformation toughening in PSZ (Stump and Budiansky, 1989a), except that λ_T and L are replaced with the *modified* quantities Λ and L_1. Thus, the overall Λs for $\rho = 0$ are obtained directly by renormalizing their old "R-curve" results in terms of the appropriate modified quantities.

In the limit $\rho \to \infty$, the particle rupture beings the instant of crack growth initiation and must be included in the stationary crack analysis as well as the growing crack calculations. Following Amazigo and Budiansky (1988), we allow the parameter $\rho \to \infty$, as the nondimensional bridge $l/L_1 \to 0$ in such a way that the product of the two factors, $\rho\sqrt{l/L_1}$, remains bounded. This special limiting process ensures that a prescribed level of Λ_p'' is maintained. The governing equations for growing cracks are formulated and then adapated to handle crack growth initiation.

In the limit $l \to 0$, the asymptotic relation

$$\operatorname{Im}\log\left(\frac{\sqrt{z}-i\sqrt{l}}{\sqrt{z}+i\sqrt{l}}\right) \approx -2\operatorname{Re}\sqrt{\frac{l}{z}} \tag{A16}$$

applies. After introducing (A16) into (A7)–(A9) and proceeding with the reformulation, we obtain the specialized equations

$$1 = \Lambda \operatorname{Re}\frac{1}{\sqrt{Z(\theta)}} - \frac{\omega}{9\pi}\int_{-\pi}^{\pi} M(\theta,\theta')\frac{\mathrm{d}}{\mathrm{d}\theta'}\left[\frac{R(\theta')\sin(\theta')}{L_1}\right]\mathrm{d}\theta' \quad \theta \leqslant \alpha \tag{A17}$$

$$\frac{3\pi}{8}[(\Lambda_p'')^2 - 1] = \Lambda\rho\sqrt{l/L_1} - \frac{2}{3\pi}(\rho\sqrt{l/L_1})^2 - \frac{\omega\rho\sqrt{l/L_1}}{9\pi}\int_{-\pi}^{\pi}\operatorname{Re}\frac{1}{\sqrt{Z(\theta)}}\frac{\mathrm{d}}{\mathrm{d}\theta}\left[\frac{R(\theta)\sin(\theta)}{L_1}\right]\mathrm{d}\theta \tag{A18}$$

and (A12), where w_f has been removed by (A15) and $M(\theta,\theta')$ is given by (A13). The elimination of the transformation contributions from (A12) and (A18) gives the quadratic equation

$$(\rho\sqrt{l/L_1})^2 + \frac{3\pi}{2}\rho\sqrt{l/L_1} - \frac{9\pi^2}{16}[(\Lambda_p'')^2 - 1] = 0 \tag{A19}$$

for the product $\rho\sqrt{l/L_1}$. The positive root of (A19) provides the relation

$$\rho\sqrt{l/L_1} = \frac{3\pi}{4}(\Lambda_p'' - 1). \tag{A20}$$

Finally, the introduction of (A20) into the K_{tip} restriction (A12), and the elimination of (A18) reduces the governing expressions to (A17) and the constraint

$$\Lambda = \Lambda_p'' + \frac{\omega}{9\pi}\int_{-\pi}^{\pi}\operatorname{Re}\frac{1}{\sqrt{Z(\theta)}}\frac{\mathrm{d}}{\mathrm{d}\theta}\left[\frac{R(\theta)\sin(\theta)}{L_1}\right]\mathrm{d}\theta \tag{A21}$$

for prescribed values of Λ_p'' and the parameter ω.

Crack growth initiation was treated first by noting that since the presence of the transformation provides no initial toughening, the integral portion of (A21) must be zero. The governing equation for the boundary of the transformed region, described by $z(\theta)$ of the form (19), was then found by setting $\Lambda = \Lambda_p''$ and enforcing (A17) in the angular interval $0 \leqslant \theta \leqslant \pi$. Solution for $R(\theta)/L_1$ was accomplished using the procedure detailed in Appendix C, Part II. Next, the growing crack was handled by solving (A17) and (A21) for $R(0)/L_1$, α, and Λ for each of a series of small growth increments $\delta a/L_1$ according to the growing crack procedure of Appendix C, Part I.

APPENDIX B: ANALYSIS FOR FINITE CRACKS

In Part I, the equations governing the growth of finite cracks are developed for finite, nonzero values of the interaction parameter ρ. In Part II, the limiting values $\rho = (0, \infty)$ are treated.

Part I: Equation development

During generalized growth, the combined effects of the applied stress σ, the transformations, and the bridging particles maintain σ_m at σ_m' just outside the active segments of both transformed regions. Simultaneously, K_{tip} and $v^+(d)$, the upper crack face displacement at the end of the right strip, are held respectively at the critical values $K_m\sqrt{1-c_p}$ and v_f. Complex stress-potential methods are used to formulate the appropriate expressions in a manner analogous to that of Appendix A. However, instead of using the potential $\phi(z)$, it is more convenient to deal with the alternate form

$$\Phi(z) = \frac{\partial \phi(z)}{\partial z} \tag{B1}$$

for the first part of the analysis. Following Stump and Budiansky (1989a), the potentials due to the applied stress σ and the transformation regions are respectively

$$\Phi_a(z) = \frac{\sigma}{2}\left[\frac{z}{\sqrt{z^2-c^2}} - \frac{1}{2}\right] \tag{B2}$$

and

$$\Phi_T(z) = -\frac{Ec_i\theta_p^T}{12\pi(1-\nu)}\oint_{C_+ + C_-} \frac{z+z_0}{\sqrt{z^2-c^2}\left(\sqrt{z^2-c^2}+\sqrt{z_0^2-c^2}\right)}\,dy_0 \tag{B3}$$

where the integral is carried out over $C_{+,-}$, the exteriors of the left and right transformed regions. Tada *et al.* (1985) list the potential for "Dugdale-like" bridging strips of strength c_pS and ends at $\pm d$ as

$$\Phi_p(z) = -\frac{c_pS}{\pi}\left\{\frac{z}{\sqrt{z^2-c^2}}\cos^{-1}\left(\frac{d}{c}\right) - \frac{i}{2}\log\left(\frac{d\sqrt{z^2-c^2}-iz\sqrt{c^2-d^2}}{d\sqrt{z^2-c^2}+iz\sqrt{c^2-d^2}}\right)\right\}. \tag{B4}$$

The branch of $\sqrt{z^2-c^2} \approx z$ as $|z| \to \infty$ is taken, and the branch cut lies along the crack faces.

We now proceed to find K_{tip} and the mean-stress exterior to the transformed regions by substituting the sum $\Phi = \Phi_a + \Phi_T + \Phi_p$ into the formulas

$$\sigma_m = \frac{4(1+\nu)}{3}\,\mathrm{Re}\,\Phi(z) \tag{B5}$$

and

$$K_{tip} = \lim_{x \to c} 2\sqrt{2\pi(x-c)}\,\Phi(x) \quad x \geqslant c. \tag{B6}$$

The resulting expressions are

$$\sigma_m = \frac{2\sigma(1+\nu)}{3}\left[\mathrm{Re}\,\frac{z}{\sqrt{z^2-c^2}} - \frac{1}{2}\right] - \frac{Ec_i\theta_p^T}{9\pi}\left(\frac{1+\nu}{1-\nu}\right)\oint_{C_+ + C_-} \mathrm{Re}\,\frac{z+z_0}{\sqrt{z^2-c^2}\left(\sqrt{z^2-c^2}+\sqrt{z_0^2-c^2}\right)}\,dy_0$$
$$-\frac{2c_pS(1+\nu)}{3\pi}\left\{2\cos^{-1}\left(\frac{d}{c}\right)\mathrm{Re}\left(\frac{z}{\sqrt{z^2-c^2}}\right) + \mathrm{Im}\log\left(\frac{d\sqrt{z^2-c^2}-iz\sqrt{c^2-d^2}}{d\sqrt{z^2-c^2}+iz\sqrt{c^2-d^2}}\right)\right\} \tag{B7}$$

and

$$K_{tip} = \sigma\sqrt{\pi c} - 2c_pS\sqrt{\frac{c}{\pi}}\cos^{-1}\left(\frac{d}{c}\right) - \frac{Ec_i\theta_p^T}{6(1-\nu)\sqrt{\pi c}}\oint_{C_+ + C_-} \mathrm{Re}\,\frac{\sqrt{z_0+c}}{\sqrt{z_0-c}}\,dy_0. \tag{B8}$$

The crack face displacement at the end of the right strip is established by integrating the potentials (B2)–(B4) with respect to z, and then substituting the resulting combination, $\phi = \phi_a + \phi_T + \phi_p$, into the formula

$$v^+(d) = \frac{2(1-\nu^2)}{E}\,\mathrm{Im}\,[\phi(d)]_-^+ \tag{B9}$$

where the brackets indicate the jump in ϕ across the crack faces. The resulting expression is

$$v^+(d) = \frac{2(1-\nu^2)}{E}\left\{\left[\sigma - \frac{2c_pS}{\pi}\cos^{-1}\left(\frac{d}{c}\right)\right]\sqrt{c^2-d^2} - \frac{2c_pS}{\pi}\,d\log\left(\frac{d}{c}\right)\right\}$$
$$-\frac{c_i\theta_p^T(1+\nu)}{3\pi}\oint_{C_+ + C_-} \mathrm{Im}\log\left(\frac{\sqrt{z_0-c}\sqrt{c+d}+i\sqrt{z_0+c}\sqrt{c-d}}{\sqrt{z_0-c}\sqrt{c+d}-i\sqrt{z_0+c}\sqrt{c-d}}\right)dy_0. \tag{B10}$$

In order to be consistent with previous formulas, the branch cuts of the terms $\sqrt{z_0 \pm c}$ lie along the negative x-axis.

The governing equation for the active-boundary segments is now formulated by allowing z to approach $z_+(\theta)$, given by (19), from the exterior of the transformed region while setting $\sigma_m = \sigma_m^c$. Simultaneously, the two constraints $K_{tip} = K_m\sqrt{1-c_p}$ and $v^+(d) = v_f$ are asserted. After introducing (1), (2), (8), and nondimensional coordinates $Z = z/L_1$, $C = c/L_1$ etc., we obtain the equations

$$1 = \frac{\sigma}{\sigma_1}\sqrt{\frac{2L_1}{a}}\left[\mathrm{Re}\,\frac{Z_+(\theta)}{\sqrt{Z_+^2(\theta)-C^2}} - \frac{1}{2}\right] - \frac{\omega}{9\pi}\int_{-\pi}^{\pi}[N_+(\theta,\theta') - N_-(\theta,\theta')]\,\mathrm{d}Y(\theta')$$

$$-\frac{2\rho}{3\pi}\left\{2\cos^{-1}\left(\frac{D}{C}\right)\mathrm{Re}\,\frac{Z_+(\theta)}{\sqrt{Z_+^2(\theta)-C^2}} + \mathrm{Im}\log\left[\frac{D\sqrt{Z_+^2(\theta)-C^2} - iZ_+(\theta)\sqrt{C^2-D^2}}{D\sqrt{Z_+^2(\theta)-C^2} + iZ_+(\theta)\sqrt{C^2-D^2}}\right]\right\} \quad \text{(B11)}$$

$$w_f = \frac{\sigma}{\sigma_1}\sqrt{\frac{C^2-D^2}{2a/L_1}} - \frac{2\rho}{3\pi}\left\{\sqrt{C^2-D^2}\cos^{-1}\left(\frac{D}{C}\right) + D\log\left(\frac{D}{C}\right)\right\} - \frac{\omega}{18\pi}\int_{-\pi}^{\pi}[Q_+(\theta) - Q_-(\theta)]\,\mathrm{d}Y(\theta) \quad \text{(B12)}$$

$$1 = \frac{\sigma}{\sigma_1}\sqrt{\frac{C}{a/L_1}} - \frac{2\rho\sqrt{2C}}{3\pi}\cos^{-1}\left(\frac{D}{C}\right) - \frac{\omega}{18\pi}\int_{-\pi}^{\pi}\mathrm{Re}\left[\frac{\sqrt{Z_+(\theta)+C}}{\sqrt{Z_+(\theta)-C}} - \frac{\sqrt{Z_-(\theta)+C}}{\sqrt{Z_-(\theta)-C}}\right]\mathrm{d}Y(\theta) \quad \text{(B13)}$$

where w_f is given by (A15),

$$N_{+,-}(\theta,\theta') = \mathrm{Re}\,\frac{Z_+(\theta)+Z_{+,-}(\theta')}{\sqrt{Z_+^2(\theta)-C^2}\left(\sqrt{Z_+^2(\theta)-C^2}+\sqrt{Z_{+,-}^2(\theta')-C^2}\right)} \quad \text{(B14)}$$

$$Q_{+,-}(\theta) = \mathrm{Im}\log\left[\frac{\sqrt{Z_{+,-}(\theta)-C}\sqrt{C+D}+i\sqrt{Z_{+,-}(\theta)+C}\sqrt{C-D}}{\sqrt{Z_{+,-}(\theta)-C}\sqrt{C+D}-i\sqrt{Z_{+,-}(\theta)+C}\sqrt{C-D}}\right] \quad \text{(B15)}$$

and

$$\mathrm{d}Y(\theta) = \frac{\mathrm{d}}{\mathrm{d}\theta}\left[\frac{R(\theta)\sin(\theta)}{L_1}\right]\mathrm{d}\theta. \quad \text{(B16)}$$

The integral equation (B11) applies in the interval $\theta \leqslant \alpha$.

Growing cracks were handled in the following manner for prescribed values of the parameters (ω, ρ, and a/L_1), the toughening ratio Λ_p^{∞}, and a set of Cs corresponding to a series of small growth increments $\delta a/L_1$. Equations (B11) and (B13), a nonlinear integral equation and a constraint, were enforced throughout crack growth to determine the nondimensional active-boundary radius $R(\theta)/L_1$ and the *modified* stress ratio σ/σ_1. During initial growth, the critical COD constraint (B12) was not enforced since the end of the segment D remained fixed at the precut tip position a/L_1. When the tip had advanced far enough that the right side of (B12) reached the critical value w_f, the constraint was turned on and D allowed to move behind the growing tips. The numerical procedure used to solve (B11)–(B13) for the unknowns $R(\theta)/L_1$, σ/σ_1, α, and D during generalized growth is discussed in Appendix C, Part I. The special modifications necessary to treat initial growth and the very first growth increment are also detailed.

Part II: Limiting values of the interaction parameter

In the limit $\rho \to 0$, bridging particles only interact with the transformations after the crack has advanced a "long" way, and the "nominal" K has begun to dominate growth. Thus, σ/σ_1 depends on just the applied stress and the transformations. Setting $\rho = 0$ in (B11) and (B13), and relaxing the constraint (B12) provides equations which are analogous to those describing transformation strengthening in PSZ (Stump and Budiansky, 1989b). Their results are easily adapted for the combined material by replacing L and σ_0 with the modified values L_1 and σ_1.

In the limit $\rho \to \infty$, particle rupture begins the instant of crack growth initiation and must be included in the stationary crack analysis as well as the growing crack treatment. We proceed in a manner analogous to that of Appendix A, Part II by developing the limiting equations for growing cracks and then specializing the results to handle crack growth initiation. In order to maintain a prescribed level of Λ_p^{∞}, we allow the parameter $\rho \to \infty$ while the bridge length $l/L_1 = C - D \to 0$ in a way such that the product of the factors $\rho\sqrt{C-D}$ remains constant. In the limit $d \to c$, the following asymptotic forms apply

$$\cos^{-1}\left(\frac{d}{c}\right) \approx \sqrt{2\left(1-\frac{d}{c}\right)} \quad \text{(B17)}$$

$$d\log\left(\frac{d}{c}\right) \approx d - c \quad \text{(B18)}$$

$$\log\left[\frac{d\sqrt{z^2-c^2} - iz\sqrt{c^2-d^2}}{d\sqrt{z^2-c^2} + iz\sqrt{c^2-d^2}}\right] \approx -2i\sqrt{2\left(1-\frac{d}{c}\right)}\,\frac{z}{\sqrt{z^2-c^2}} \quad \text{(B19)}$$

$$\log\left[\frac{\sqrt{z_0-c}\sqrt{c+d}+i\sqrt{z_0+c}\sqrt{c-d}}{\sqrt{z_0-c}\sqrt{c+d}-i\sqrt{z_0+c}\sqrt{c-d}}\right] \approx i\sqrt{2\left(1-\frac{d}{c}\right)}\,\frac{\sqrt{z_0+c}}{\sqrt{z_0-c}}. \quad \text{(B20)}$$

By introducing (B17)–(B20) into (B7), (B8), and (B10), and then reformulating, we derive the specialized equations

$$1 = \frac{\sigma}{\sigma_1}\sqrt{\frac{2L_1}{a}}\left[\mathrm{Re}\,\frac{Z_+(\theta)}{\sqrt{Z_+^2(\theta)-C^2}} - \frac{1}{2}\right] - \frac{\omega}{9\pi}\int_{\pi}^{\alpha}[N_+(\theta,\theta') - N_-(\theta,\theta')]\frac{\mathrm{d}}{\mathrm{d}\theta'}\left[\frac{R(\theta')\sin(\theta')}{L_1}\right]\mathrm{d}\theta' \quad \theta \leqslant \alpha \tag{B21}$$

$$\frac{3\pi}{8}\frac{(\Lambda_p^n)^2-1}{\rho\sqrt{C-D}} = \frac{\sigma}{\sigma_1}\sqrt{\frac{C}{a/L_1}} - \frac{2}{3\pi}(\rho\sqrt{C-D}) - \frac{\omega}{18\pi}\int_{-\pi}^{\alpha}\mathrm{Re}\left[\frac{\sqrt{Z_+(\theta)+C}}{\sqrt{Z_+(\theta)-C}} - \frac{\sqrt{Z_-(\theta)+C}}{\sqrt{Z_-(\theta)-C}}\right]\frac{\mathrm{d}}{\mathrm{d}\theta}\left[\frac{R(\theta)\sin(\theta)}{L_1}\right]\mathrm{d}\theta \tag{B22}$$

and

$$1 = \frac{\sigma}{\sigma_1}\sqrt{\frac{C}{a/L_1}} - \frac{\omega}{18\pi}\sqrt{\frac{2}{C}}\int_{-\pi}^{\alpha}\mathrm{Re}\left[\frac{\sqrt{Z_+(\theta)+C}}{\sqrt{Z_+(\theta)-C}} - \frac{\sqrt{Z_-(\theta)+C}}{\sqrt{Z_-(\theta)-C}}\right]\frac{\mathrm{d}}{\mathrm{d}\theta}\left[\frac{R(\theta)\sin(\theta)}{L_1}\right]\mathrm{d}\theta \tag{B23}$$

where (A15) has been used to fix the left side of (B22), and $N_{+,-}(\theta,\theta')$ is given by (B14). The elimination of the transformation terms from (B22) and (B23) gives the quadratic equation

$$(\rho\sqrt{C-D})^2 + \frac{3\pi}{2}(\rho\sqrt{C-D}) - \frac{9\pi^2}{16}((\Lambda_p^n)^2-1) = 0 \tag{B24}$$

for the product $\rho\sqrt{C-D}$. The positive root yields the relation

$$\rho\sqrt{C-D} = \frac{3\pi}{4}(\Lambda_p^n - 1) \tag{B25}$$

which corresponds directly to (A20), the comparable expression for semi-infinite cracks. Finally, the substitution of (B25) into the K_{tip} condition (B23) and the elimination of (B22) reduces the governing equations to the nonlinear integral equation (B21) and the constraint

$$\Lambda_p^n = \frac{\sigma}{\sigma_1}\sqrt{\frac{C}{a/L_1}} - \frac{\omega}{18\pi}\sqrt{\frac{2}{C}}\int_{\pi}^{\alpha}\mathrm{Re}\left[\frac{\sqrt{Z_+(\theta)+C}}{\sqrt{Z_+(\theta)-C}} - \frac{\sqrt{Z_-(\theta)+C}}{\sqrt{Z_-(\theta)-C}}\right]\frac{\mathrm{d}}{\mathrm{d}\theta}\left[\frac{R(\theta)\sin(\theta)}{L_1}\right]\mathrm{d}\theta \tag{B26}$$

for prescribed Λ_p^n, ω, and a/L_1.

The special situation of crack growth initiation was handled first by setting the applied stress ratio σ/σ_1 and C equal to the "initiation" values σ_i/σ_1 and a/L_1. The boundaries of the transformed regions were described by (18) and the integral equation (B21) was extended to cover the full angular interval $0 \leqslant \theta \leqslant \pi$. The constraint (B26) remaind in effect. The solution procedure for $R(\theta)/L_1$ and σ_i/σ_1 is described in Appendix C, Part II. An analysis revealed that in order for the transformed region to remain finite-sized for all $\omega \geqslant 0$, the parameter a/L_1 needed to be restricted to values *greater* than $(\Lambda_p^n)^2/2$. Next, growing cracks were handled by using the solution procedure described in Appendix C, Part I to solve (B23) and (B26) for $R(\theta)/L_1$, σ/σ_1, and a set of Cs corresponding to a series of finite growth increments.

APPENDIX C: NUMERICAL ANALYSIS

Part I of this appendix describes the numerical solution to the systems of equations governing growing semi-infinite and finite cracks. Part II describes the solution procedure for crack-growth initiation in the limit $\rho \to \infty$.

Part I: Growing cracks

The system of equations consists of an integral equation for the function $R(\theta)/L_1$, the current active-boundary segment, and a variety of constraints for several scalar unknowns. Two scalars, the angle α marking the end of the current active segment and the appropriate "resistance ratio" (i.e. Λ for semi-infinite cracks or σ/σ_1 for finite cracks), must be found during every growth increment. When the crack is in generalized growth and ρ is finite, the critical COD constraint must be added to determine the strip end, l/L_1 or D. Finally, during the very first growth increment, an additional unknown angle β must be introduced to determine the passive segment connection with the transformed region(s) surrounding the stationary crack tip(s).

Rather than describe each solution procedure for all possible circumstances, we discuss the general approach used to solving a system containing the boundary integral equation and M constraint equations for the function $R(\theta)/L_1$ and M scalar unknowns. The special treatment of the very first growth increment is discussed at the end of this part.

The function $R(\theta)/L_1$ for the active-boundary radius was expanded in the finite series

$$R(\theta)/L_1 = \sum_{n=0}^{N} a_n T_{2n}(\theta/\alpha) \quad 0 \leqslant \theta \leqslant \alpha \tag{C1}$$

where the Ts are Tchebyshev polynomials of the first kind and the a_ns are $N+1$ unknown coefficients. The expansion (C1) was substituted into the system, and the integral equation was collocated at the $N+1$ points $\theta_j = j\alpha/N$ $(j = 0, \ldots, N)$. An equation for the angle α was generated by asserting the tangency condition

$$\left.\frac{dY(x)}{dX}\right|_{active} = \left.\frac{dY}{dX}\right|_{passive} \tag{C2}$$

at the junction of the active and passive segments. The final system consisted of $N+M+1$ equations in the $N+M+1$ unknowns $(a_0, \ldots, a_N, x, \Lambda, [l\ L_1])$. (Here variables for the semi-infinite crack have been used, and the bracket notation indicates that the quantity may be an active unknown.) Solution was accomplished by using a Newton–Raphson iterative procedure with convergence specified by a relative change of less than 0.1% in each of the unknowns between iterations. All integrals were broken up into sub-intervals along the active-passive-residual segments and were evaluated by separate Gauss quadrature procedures.

For the very first increment of crack growth, the passive-residual juncture needed to be located. This was accomplished by introducing the unknown angle β to describe the juncture relative to the stationary crack, see Fig. 5. An additional tangency constraint

$$\left.\frac{dY(\beta)}{dX}\right|_{residual} = \left.\frac{dY}{dX}\right|_{passive} \tag{C3}$$

was added to the system. After the first increment, β remained fixed and aided in evaluating the integrals over the boundary during the subsequent growth increments.

It was found that five term expansions for the radius gave rapid convergence. The accuracy of select results for a specified set of growth increments was checked by repeating the calculations with the increment sizes halved. Few if any changes were observed. Typically, the starting growth increments needed to be small [i.e. less than about 0.1 times the frontal extension, $R(0)/L_1$, of the stationary transformed zones] in order to capture the rapid initial toughness increase. As the toughness peak was passed through, increment sizes could be increased.

Part II: Crack-growth initiation for $\rho \to \infty$

The specialized analysis for the transformed region(s) surrounding the crack tip(s) at the instant of crack-growth initiation is discussed. For both finite and semi-infinite cracks, a nonlinear integral equation for the radius vector $R(\theta)/L_1$ must be enforced in the angular interval $0 \leqslant \theta \leqslant \pi$. For the finite crack, there is an additional constraint equation for the "initiation" stress ratio σ_i/σ_1. We describe the solution procedure for the finite crack.

The boundary radius vector was expanded in the finite series

$$R(\theta)/L_1 = \sum_{n=0}^{N} a_n \cos(n\theta) \quad 0 \leqslant \theta \leqslant \pi \tag{C4}$$

which meets the appropriate symmetry conditions (Stump and Budiansky, 1989a). The expression (C4) was substituted into (B21) and (B26). Next, the integral equation (B21) was collocated at the $N+1$ points $\theta_j = j\pi/N$ $(j = 0, \ldots, N)$ to yield $N+2$ equations in the unknowns $(a_0, \ldots, a_N, \sigma_i/\sigma_1)$. All integrals were evaluated by Gauss quadrature. A Newton Raphson iterative procedure was used to obtain a solution with convergence specified by a relative change of less than 0.1% in each of the unknowns between iterations. Typically, 10 term expansions for the radius gave rapid convergence. The equation (A21) for the semi-infinite crack was treated in a similar manner. The expansion (C4) was substituted into the integral equation, and the collocation and Newton–Raphson procedures described above were used to obtain a solution for the coefficients.